Monthly Notices
of the
ROYAL ASTRONOMICAL SOCIETY

MNRAS **447,** 3467–3474 (2015) doi:10.1093/mnras/stu2655

Simulation of atmospheric turbulence phase screen for large telescope and optical interferometer

Peng Jia,[1]★ Dongmei Cai,[1] Dong Wang[1] and Alastair Basden[2]

[1]*College of Physics and Optoelectronics, Taiyuan University of Technology, Taiyuan 030024, China*
[2]*Department of Physics, University of Durham, South Road, Durham DH1 3LE, UK*

Accepted 2014 December 12. Received 2014 November 18; in original form 2014 October 16

ABSTRACT

As the pupil size of ground-based telescopes increases, adaptive optics systems become more and more important for almost all astronomical observations. To test the performance of adaptive optics systems through simulation and with test bench experiments, we need to model the atmospheric turbulence with high fidelity. To fulfil this goal, a new method based on optimal sampling with a sparse spectrum model is discussed. This method can effectively simulate the atmospheric phase screen of any power spectrum with a controllable error budget.

Key words: atmospheric effects – instrumentation: adaptive optics – instrumentation: interferometers.

1 INTRODUCTION

Atmospheric turbulence is a serious limitation for ground-based optical–infrared observations. Due to distorted wavefronts brought by atmospheric turbulence, the angular resolution of telescopes is independent of their pupil size and is limited to an equivalent telescope diameter of about 10 cm (Roddier 1981). There are several techniques that can be used to reduce the perturbing effect brought by the atmospheric turbulence: with adaptive optics (AO), it is possible to obtain the full potential in angular resolution of ground-based observations (Babcock 1953). Because of the outstanding performance improvements, AO systems are commonly considered for installation on modern telescopes (Dekany et al. 2004; Lloyd-Hart et al. 2006; Markus 2010), including interferometric telescopes, to increase their observation abilities allowing scientific goals to be met (Bonaccini et al. 1998; ten Brummelaar et al. 2012). As telescope diameter increases, the design of an AO system becomes increasingly complicated, and to reduce overall cost and maximize performance, simulation of AO systems is essential during their development (Carbillet et al. 2004; Jolissaint, Véran & Conan 2006; Basden et al. 2007). Because AO systems are used to correct the wavefront phase error introduced by the atmospheric turbulence, it is important to verify AO system performance using realistic working conditions (Basden 2014). A key part of an end-to-end AO simulation is that of the distorted wavefronts introduced by atmospheric turbulence. During simulations, atmospheric turbulence is divided into discrete uncorrelated layers at different heights above the ground, according to user specifications, requirements and *in situ* test results (Arcidiacono et al. 2004). Then using a Monte Carlo method, these different atmospheric turbulent layers will be generated with unique parameters such as inner and outer scale. The typical distribution of layers in the atmosphere, and the turbulent strength of these layers can be obtained through site measurement. For high-fidelity simulations, it is important to choose a method of phase screen generation that has a controllable error budget. However, this is not an easy task because atmospheric turbulence is a highly non-linear process.

There are several methods that can be used to simulate an atmospheric phase screen, such as the Fourier series-based method (Lane, Glindemann & Dainty 1992; Frehlich 2000; Sedmak 2004), the covariance matrix method (Harding, Johnston & Lane 1999; Assémat, Wilson & Gendron 2006), the Zernike polynomial method (Roddier 1990; Hu et al. 2006), the stochastic model (Beghi, Cenedese & Masiero 2008), the fractal interpolation method (Wu et al. 2009) and extrapolation method (Jia & Zhang 2012). These methods divide the atmospheric turbulence phase screen into discrete orthogonal bases with random coefficients that satisfy particular statistical characteristics, such as Zernike polynomials and coefficients in Zernike polynomial method, harmonics and frequency components in Fourier series-based method, phase values at discrete points and correlation parameters in the covariance matrix and fractal methods. The input model coefficients are not completely random but are obtained from the atmospheric turbulence model and site testing data (Charnotskii 2013). A commonly accepted model of atmospheric turbulence is the Kolmogorov model (Frisch 1995), which is based on a statistical description of refractive index. The Kolmogorov model shows that the power spectrum of the atmospheric turbulence follows a $\kappa^{-3/5}$ law in the inertial range which means that low-frequency components have more energy than higher ones. The characteristic of this model demands more sample points at lower frequency bands than in higher frequency bands during simulation. This property brings serious limitations to the standard fast Fourier transform

★E-mail: robinmartin20@gmail.com

(FFT) based method, because sample points are distributed uniformly for an FFT (Bracewell 1986). Several methods are proposed to compensate loss of the low-frequency components, such as the sub-harmonic addition method (Recolons & Dios 2005; Xiang 2012), a hybrid method (Xiang 2014), or the polar-logarithmic spectrum sampling method (Burckel & Gray 2013; Cai et al. 2014). Simulation results indicate that these methods are effective and that phase error is reduced. However, it is interesting to consider whether an optimal number of sub-harmonics or samples exists for a given computational cost and simulation fidelity. Carbillet and Riccarid gave an accurate analytical result of how many sub-harmonics are required in simulation (Carbillet & Riccardi 2010). Compared with their results, the choice of polar-logarithmic spectrum sampling is somewhat arbitrary. According to the sparse spectrum model of turbulence phase screens (Charnotskii 2013), atmospheric turbulence can be modelled as a 2D random field of wavefront phase as a sum of harmonics with arbitrary frequencies. Therefore, if it is possible to obtain the optimal sample sequence with a given error budget, then it is possible to simulate the phase screen with a controllable error. We will introduce the concept of the error budget in Section 2 and compute the optimal sample points for the Kolmogorov model in Section 3.

The Kolmogorov spectrum is a widely used atmospheric turbulence model. However, other studies have found significant deviations from Kolmogorov statics when the aperture of telescopes increases (Tokovinin, Sarazin & Smette 2007; Maire et al. 2008). For modern telescopes with diameters of dozens of metres and interferometers with dozens to hundreds of metres, a different spectrum model is required (Martinez et al. 2010). A common choice is the Von Kármán spectrum (Tatarskii 1961; Ziad et al. 2000), which introduces an additional parameter, the outer scale beyond which wavefronts are uncorrelated. Whether this model is accurate is still an open question, but it is commonly accepted that the true atmospheric power spectrum does indeed deviate from the Kolmogorov spectrum. There are also other generalized modified atmospheric spectrum models for non-Kolmogorov turbulence (Xue et al. 2011). A lack of ample site characterisation and testing results means that spectrum models for different sites at different scales may be different from the commonly accepted spectrum models and may not have an analytical formulation. Under these conditions, a new simulation method which can simulate the atmospheric turbulence of an arbitrary spectrum with controllable error budget is required. Based on the optimal sample method and spectrum decomposition model, a new simulation method will be discussed in Section 4. In Section 5, we will discuss applications of this simulation method in real-time simulation and laboratory test. Conclusions are given in Section 6.

2 THE ERROR OF AN ATMOSPHERIC TURBULENCE PHASE SCREEN BASED ON THE SPARSE SPECTRUM MODEL

The phase screen induced by the atmospheric turbulence is a random process with zero mean and is a mean-square continuous wide-sense stationary (WSS) process within a locally homogenous and isotropic domain. The WSS process can be expressed as Fourier–Stieltjes integral:

$$\phi(\boldsymbol{x}) = \int_{u_i}^{u_o} \mathrm{e}^{j2\pi u x} \mathrm{d}Z(\boldsymbol{u}), \tag{1}$$

where u_o and u_i are the upper and lower limits of the frequency band, and $Z(\boldsymbol{u})$ is random spectrum function of $\phi(\boldsymbol{x})$ for frequency band $\boldsymbol{u}$ in point $\boldsymbol{x}$. It has the following properties:

$$\begin{aligned} E[\mathrm{d}Z(\boldsymbol{u})] &= 0, \\ E[\mathrm{d}Z(\boldsymbol{u})\mathrm{d}Z^*(\boldsymbol{v})] &= 0, \qquad \boldsymbol{u} \neq \boldsymbol{v} \\ E[|\mathrm{d}Z(\boldsymbol{u})|^2] &= \Phi_\phi(\boldsymbol{u})d\boldsymbol{u}, \end{aligned} \tag{2}$$

where $\Phi_\phi(\boldsymbol{u})$ is the power spectrum density of $\phi(\boldsymbol{u})$ at the point $\boldsymbol{u}$, and $E[]$ denotes the expectation operator. An equivalent expression for discrete form with random spectrum components has also been presented (Charnotskii 2013). For real applications, the sample points and the points in the phase screen are discrete, and here we choose the Cartesian coordinate and harmonics:

$$\phi(x, y) = \sum_{u=u_1}^{u_n} \sum_{v=v_1}^{v_n} \mathrm{e}^{j2\pi(xu+yv)} \cdot c(u, v), \tag{3}$$

where $c(u, v)$ is the random complex amplitude, with this equation representing the relative weight of different frequency components. It satisfies

$$\begin{aligned} E[c(u, v)] &= 0, \\ E[c(u_1, v_1) \cdot c^*(u_2, v_2)] &= 0, \ u_1 \neq u_2 \ or \ v_1 \neq v_2 \\ E[|c(u, v)|^2] &= \Phi_\phi(u, v) \cdot \Delta(u, v). \end{aligned} \tag{4}$$

According to equation (3), the frequency sequence is uniformly sampled and can be expressed as series sum in a square grid for the FFT-based method. Equation (3) is recursive and the algorithm complexity is $n \cdot n$ for each point. However, because the sample points distribute uniformly for the FFT-based method, it can be transformed into an iterative structure with a reduced complexity of $n \cdot \log(n)$. The high speed and the simple form of the FFT-based method make it the most popular method in simulation of atmospheric turbulence phase screens. However, this method suffers from a lack of low-frequency components brought by insufficient sampling points in the low-frequency band when it is used to simulate phase screens with a Kolmogorov spectrum. Several methods have been proposed to compensate this error, but are only proven to be effective for Kolmogorov phase screens, and it is unknown whether these methods are also effective for phase screens with other statistical properties. We can calculate the error in different atmospheric turbulence phase screens with different spectrums and sampling methods. According to equation (3), the value of the phase screen at one point can be viewed as a sum of different frequency components. The frequency components may be chosen arbitrarily according to our requirements: it is clear that if there are an infinite number of sample points, every component will be well presented and the error will become infinitely small. Unfortunately, this is impractical because of the huge computation resources required. With limited sample points, there are inevitable errors during the simulation, brought mainly by the discretization of the power spectrum. Theoretically, the energy in the frequency band u_1 between u_0 and u_2 can be expressed as

$$\mathrm{Energy}(u_1) = \int_{u_0}^{u_2} [\Phi_\phi(u)]^{0.5} \mathrm{d}u. \tag{5}$$

Because of the discretization of the power spectrum, the energy in the frequency band u_1 between u_0 and u_2 is expressed as

$$\mathrm{DisEnergy}(u_1) = [\Phi_\phi(u_1)]^{0.5} \cdot (u_2 - u_0), \tag{6}$$

where u_0, u_1, and u_2 are three nearby sample points. The difference between Energy(u) and DisEnergy(u) will be brought into all the

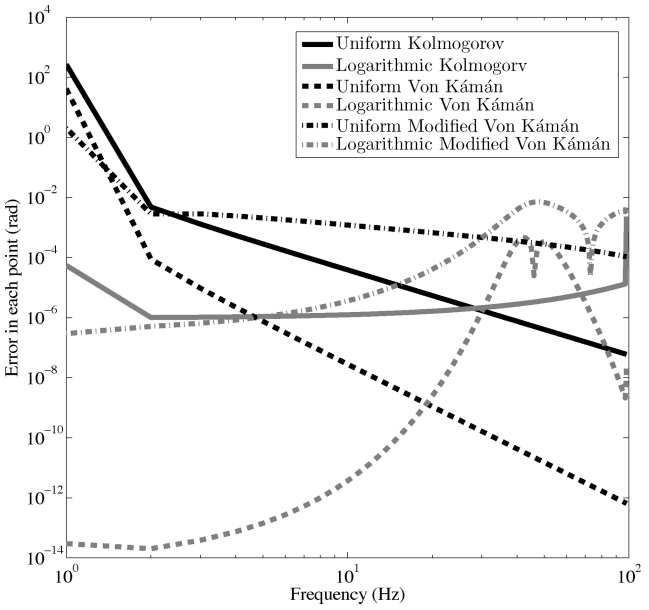

Figure 1. Phase screen errors in each point of different bands for different sample methods. The number of sample points is 1000 for uniform sampling and logarithmic sampling. It can be deduced that the logarithmic sampling method is better than the Kolmogorov spectrum because the error in frequency band is lower, between 10^{-4} and 10^{-6} rad. The logarithmic sampling method is not adequate for the Von Kármán spectrum because the error is not uniformly distributed across the whole band. It is better to readjust the positions of sample points from low bands to high bands.

points of the phase screen during the simulation. We define the error of each point in the frequency band u_1 as

$$\text{EnergyError}(u_1) = \frac{\text{Energy}(u_1) - \text{DisEnergy}(u_1)}{\text{totalpoints}/u_1}, \tag{7}$$

where totalpoints stands for the number of the points along the sample direction. The error function defined in equation (7) can be used to evaluate different sample methods for different spectrums as shown in Fig. 1. The uniform sampling method and logarithmic sampling method are defined as follows:

Uniform sampling :

$$u(n) = u_{\min} + (u_{\max} - u_{\min}) \cdot \frac{n-1}{N-1},$$

logarithmic sampling :

$$u(n) = u_{\min} \cdot \left(\frac{u_{\max}}{u_{\min}}\right)^{\frac{n-1}{N-1}}, \tag{8}$$

where N is the total sample points, and $u_{\min}$ and $u_{\max}$ are the lower and upper bound of the sample points, respectively. According to Carbillet and Riccarid's work (Carbillet & Riccardi 2010), the lower bound is $1/(1000 \cdot L_0)$ and according to Nyquist–Shannon sampling theorem the upper bound is $2 \cdot \text{totalpoints}/L$ where totalpoints and L are the total number of the points and the length of the phase screen. We simulate the Kolmogorv spectrum, the Von Kármán spectrum and the modified Von Kármán spectrum defined by equation (9), where r_0 is the coherent length, and u_i and u_o are defined by the inner and outer scale. It is evident that for different spectrum models the error in each point is different under different sample methods, and there does not exist a universal sample method that is effective for all spectrum models:

Kolmogorov:

$$\Phi_\phi(u) = 0.023 \cdot r_0^{-5/3} \cdot u^{-11/3}$$

Von Kármán :

$$\Phi_\phi(u) = 0.0299 \cdot r_0^{-5/3} \cdot (u^2 + u_i^2)^{-11/6}$$

Modified Von Kármán:

$$\Phi_\phi(u) = 0.0299 \cdot r_0^{-5/3} \cdot \frac{\exp(-u^2/u_o^2)}{(u^2 + u_i^2)^{11/6}}. \tag{9}$$

3 THE OPTIMAL SAMPLING METHOD FOR PHASE SCREEN GENERATION

According to Section 2, the error brought by the sparse spectrum model of a phase screen is inevitable, and distribution characteristics of the error is different for each spectrum model and sampling method. Based on the expression of error in equation (7), we can obtain a different sampling list according to our desire to maintain a low overall error. A rational approach is the redistribution of the sample points to keep all the error budget within a certain range (as an analogy, consider the aberration balancing between different fields of view in optical design; Fischer, Tadic-Galeb & Yoder 2008). The error budget depends on desired accuracy which can be defined before simulation. In addition to the error budget, the length of the phase screen, the number of points along the phase screen, the coherence length, the spectrum model and other parameters are all known inputs for a given simulation. The optimal sampling method optimizes the number of required sample points and their positions, which can be viewed as a finite energy interpolation problem. The analytical solution can be obtained through Hilbert space optimization (Potter & Arun 1989) if the spectrum model has an analytical expression. But real spectrum models may be non-analytical. To keep our sampling method universal to any spectrum model type, we therefore apply a golden section search technique (Sun & Yuan 2006). This is the limit of a Fibonacci search method when the distances of the triples of points evaluated in the algorithm form a golden ratio (the golden ratio is 0.618). The pseudo-code is given in algorithm 1. With this algorithm, we can obtain an optimal sampling list for different spectrums. Fig. 2 shows the errors of the optimal sample list and logarithmic sampling list for the Kolmogorov spectrum and Von Kármán spectrum, and Fig. 3 shows positions of the sampling points along the power spectrum density as defined in equation (9). It is evident that sampling points for simulations of phase screens with Kolmogorov and Von Kármán spectrum are different. For phase screens with a Kolmogorov spectrum, more sampling points are required in low-frequency band. For phase screens with a Von Kármán spectrum, more sampling points are required in the middle frequency band where the slope of the power spectrum density changes rapidly.

4 ATMOSPHERIC TURBULENCE SIMULATION WITH OPTIMAL SAMPLING

With the optimal sampling method introduced here, it is possible to simulate atmospheric phase screens with a controllable error budget using a sparse spectrum model. The simulation steps are different here from the traditional method as shown in algorithm 2. We define the upper and lower error bounds according to the simulation requirements. With the optimal sampling method, the sample

Algorithm 1 Finding the sample points for KL spectrum through the golden search method.

Require:
u_m Low-frequency sampling limit
u_M High-frequency sampling limit
eru Upper error bound
erd Lower error bound
step search step
tpn Number of the points along the phase screen
$ERF(u_0, u_1, u_2, tpn)$ Sample Error in u_1

Ensure: Sampling list *Sl*
Initialization
$u_0 \leftarrow u_m$
$u_2 \leftarrow (1 + step)^2 \cdot u_0$
$u_1 \leftarrow 0.618 \cdot u_2 + 0.382 \cdot u_0$
Search for the sample points in frequency band
while $u_2 \leq u_M$ **do**
  if $ERF(u_0, u_1, u_2, tpn) \leq erd$ **then**
    $u_2 \leftarrow u_2 \cdot (1 + step)$
    $u_1 \leftarrow 0.618 \cdot u_2 + 0.382 \cdot u_0$
  else if $ERF(u_0, u_1, u_2, tpn) \geq eru$ **then**
    $u_2 \leftarrow u_2/(1 + 0.1 \cdot step)$
    $u_1 \leftarrow 0.618 \cdot u_2 + 0.382 \cdot u_0$
  else
    $u_{10} \leftarrow u_0 + 0.382 \cdot (u_2 - u_0)$
    $u_{20} \leftarrow u_0 + 0.618 \cdot (u_2 - u_0)$
  end if
  for $k = 1 \rightarrow 10$ **do**
    if $ERF(u_0, u_10, u_2, tpn) \leq ERF(u_0, u_20, u_2, tpn)$ **then**
      $u_{20} \leftarrow u_1 + 0.618 \cdot (u_2 - u_{10})$
    else
      $u_{10} \leftarrow u_1 + 0.382 \cdot (u_{20} - u_1)$
    end for
    $Sl = u_{10} + 0.618 \cdot (u_{20} - u_{10})$
    $u_0 \leftarrow u_1$
    $u_2 \leftarrow u_2 \cdot (1 + step)$
    $u_1 \leftarrow 0.618 \cdot u_1 + 0.382 \cdot u_0$
end while

list can then be calculated and the phase screen will then be simulated through the sparse spectrum model with this sample list. According to equation (7), it is evident that the sample list will be different for different spectrum models and error budgets. Results from simulations of the Kolmogorov spectrum using the FFT-based method, the logarithmical sampling method, and the optimal sampling method are shown in Fig. 4. The results indicate that the optimal sampling method can simulate a phase screen with controllable error over the whole band which is particularly useful for the simulation of very long phase screens.

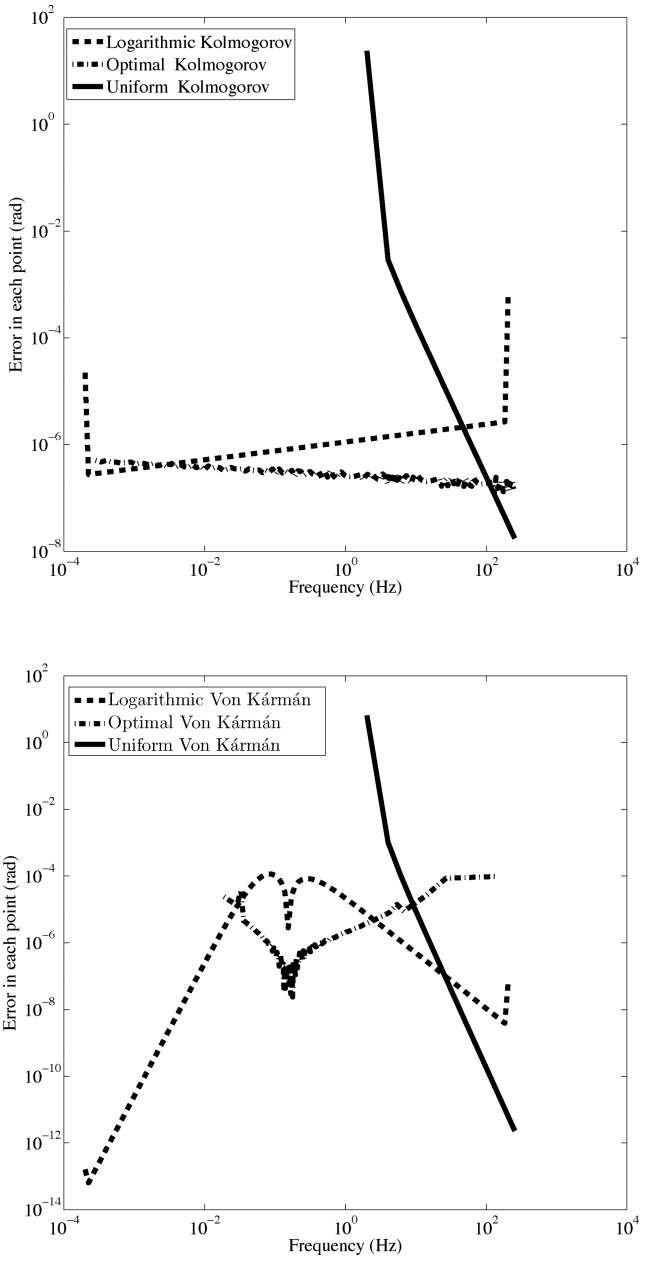

Figure 2. The sampling lists and the error of these lists for the Kolmogorov spectrum and the Von Kármán spectrum. For the Kolmogorov spectrum, the number of the sampling points of the uniform sampling and the logarithmical sampling is 128 and the number of the optimal sampling points is 149 with an error budget below 10^{-6} rad. For the Von Kármán spectrum, the error mainly lies in the middle frequency band (near $1/L_0$). The sampling points are redistributed into the middle frequency band and the error budget is below 10^{-4} rad. The number of sampling points for the Von Kármán spectrum is 128 for the uniform and logarithmical sampling and 131 for the optimal sampling.

5 REAL APPLICATIONS OF THE ATMOSPHERIC TURBULENCE PHASE SCREEN SIMULATION

The real applications of the atmospheric turbulence phase screen include two situations: for Monte Carlo simulations of AO systems and for laboratory testing of AO systems. During Monte Carlo simulations, the atmospheric turbulence phase screens will be generated in real time and with infinite length. For the laboratory test of AO systems, phase screens are etched into the fused silica or commands directly sent to liquid crystal spatial light modulators (SLM) to simulate the phase distortions. Thanks to the controllable error budget of our method, the simulation of the atmospheric phase screens can be modified according to different input requirements.

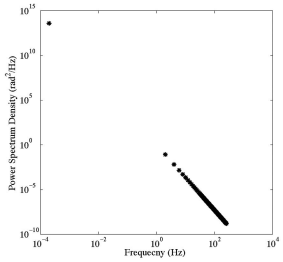

(a) Positions of sampling points for a Kolmogorov spectrum with uniform sampling

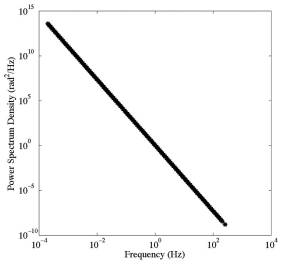

(b) Positions of sampling points for a Kolmogorov spectrum with logarithmic sampling

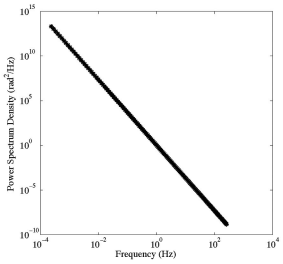

(c) Positions of sampling points for a Kolmogorov spectrum with optimal sampling

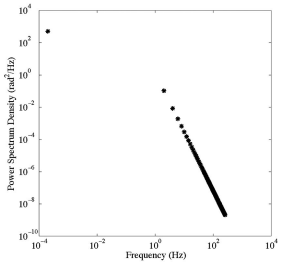

(d) Positions of sampling points for a Von Kármán spectrum with uniform sampling

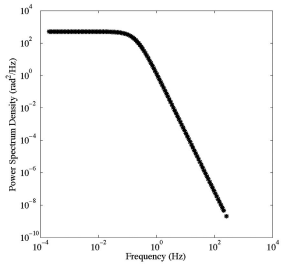

(e) Positions of sampling points for a Von Kármán spectrum with logarithmic sampling

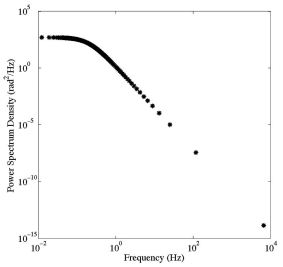

(f) Positions of sampling points for a Von Kármán spectrum with optimal sampling

Figure 3. Positions of sampling points for different spectrums and sampling methods. For the Kolmogorov spectrum, the optimal sample method redistributes the sampling points in the low- and high-frequency bands to keep the error within the error budget. For the Von Kármán spectrum, the optimal sample method redistributes the sampling points across the whole frequency band: more sampling points are added in the band where the slope of the power spectrum density changes most rapidly. The optimal sampling method indicates that to simulate Von Kármán phase screens, more points are required in the middle frequency band than in the low-frequency band, which is different from phase screens with Kolmogorov spectrum.

Algorithm 2 Framework of atmospheric turbulence phase screen simulation with the optimal sampling.

Require: Parameters of the atmospheric turbulence from site testing (r_0,L_0, spectrum model, etc.), **B**; Parameters of the simulation (error budget, size, etc.), **F**;
Ensure: Obtaining the phase screen, Φ;
1: Obtaining the sampling list **P** according to **B** and **F**
2: Calculating the coefficients $c(u, v)$ in each frequency band of the sample list **P**
3: Evaluating the value in point (x, y) in the phase screen with $c(u, v)$ and **P**
4: **return** the phase value $\Phi(x, y)$ in point (x, y)

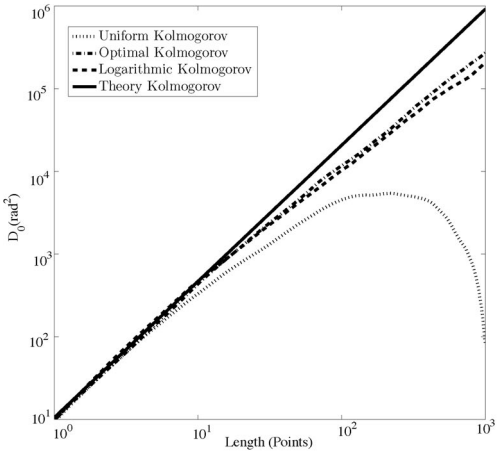

(a) Phase structure function D_0 versus the sampling frequency for the phase screens generated using different sampling methods and the sparse spectrum model.

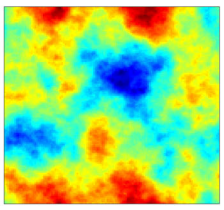

(b) One of the phase screens generated by the uniform sampling method and sparse spectrum model.

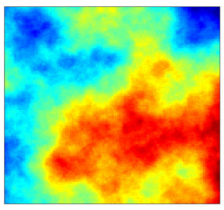

(c) One of the phase screens generated by the logarithmical sampling method and sparse spectrum model.

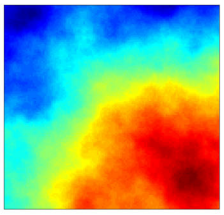

(d) One of the phase screens generated by the optimal sampling method and sparse spectrum model.

Figure 4. Simulation results comparing a uniform sampling list, a logarithmical sampling list and the optimal sampling list are compared in this figure. The number of the sampling points in the uniform and logarithmical sampling is 128, while the optimal sampling method uses 149 points. The optimal sampling method increases the low-frequency component by adding more sampling points in the low-frequency band and the results of the optimal sampling points are better than the other methods.

5.1 Atmospheric turbulence simulation for the Monte Carlo simulation of AO systems

Monte Carlo simulation of AO systems require very long phase screens which are propagated across the telescope pupil, allowing time-averaged AO system performance estimates to be obtained. The width of the phase screens is defined by the diameter of the telescope D and the ratio between the simulation and the real physical size (N pixels represent 1 m in the simulation). For a telescope

with a diameter of 30 m and moderate site conditions ($r_0 = 0.1$ m) 50 spatial sampling points per metre is adequate, leading to a phase screen width of 1500 points. This is computationally intensive, with requirements increasing when interferometric baselines are considered: if the length of the baseline for the interferometer is 300 m, this will then require 15 000 spatial sampling points. There are two methods to accelerate the simulation speed and reduce the computational cost: if the width of the phase screen is not too large, we will interpolate an oversampled FFT to get the phase screen, an approach identical to the method applied in the non-uniform FTT of type two (Greengard & Lee 2004). Because the phase screen is generated iteratively, the value of each sample point can be directly obtained from the coefficients in different frequency bands. If the width of the phase screen is large enough, we will store the coefficient matrix and calculate the value of the points using parallel computation, leading to a large increase in simulation speed. A graphics processing unit (GPU) typically has thousands of cores and is an ideal technology for phase screens computation. If we want to simulate the phase screen for interferometric telescopes, we only need to evaluate the values of points in the telescopes which will decrease the computational requirements.

Another problem for Monte Carlo simulations lies in the length of the phase screen: the atmospheric turbulence generated with a sparse spectrum method has a finite length. Several methods have been proposed to increase the length of phase screens. According to Vorontsov et al. (2008), a long phase screen can be generated through addition of different phase screens (with the same statistical properties) as

$$\phi_\infty(x, y) = \sum_{j=0}^{+\infty} \psi_j(x)\phi_j(x - j, y), \tag{10}$$

where ϕ_j is j independent phase screens and ψ is a *splicing* function that is used to keep the second-order statistical properties close to the theoretical model when the phase screen is smaller than L_0. In Vorontsov's paper, a detailed discussion about choice of the *splicing* function was given and a trigonometric function used for simplicity. When the phase screen is longer than L_0, a new *splicing* function is required. For our applications, the length of phase screen is much longer than L_0, and an appropriate simple *splicing* function is that of a top-hat function modified by the cosine function as

$$\psi_j(x) = \begin{cases} \left|\cos(\frac{\pi x}{2(p-0.5\cdot L_0)})\right|, & x \in [-p, -0.5L_0] \cup [0.5L_0, p], \\ 1, & x \in [-0.5L_0, 0.5L_0], \\ 0, & x \notin [-p, p], \end{cases} \tag{11}$$

where $2p$ is the length of the phase screen and L_0 is the length of the outer scale in the phase screen. This *splicing* function can combine statistically independent phase screens together and generate phase screens with a required greater length. The correlation function of phase screen ϕ_∞ is

$$\begin{aligned} &\mathrm{Cov}_{\phi_\infty}(x_0, y_0, x_0 + x, y_0 + y) \\ &\quad = \mathrm{Cov}_\phi(x, y) \sum_{j=0}^{+\infty} \psi_j(x_0)\psi_j(x_0 + x). \end{aligned} \tag{12}$$

To keep the results close to the second-order statistical properties predicted by theory, the *splicing* function has to satisfy three conditions. First the *splicing* function should be positive. Secondly, the variance of ψ and ψ_∞ should be equal which means $\mathrm{Cov}_{\phi_\infty}(x_0, y_0, x_0, y_0) = \mathrm{Cov}_\phi(0, 0)$. Thirdly, the difference between the correlation functions of the long phase screen and that of the independent phase screen should be relatively small. These conditions can be expressed as

$$\psi_j(x_0) \geq 0$$

$$\sum_{j=0}^{+\infty} \left[\psi_j(x_0)\right]^2 = 1$$

$$\left|\mathrm{Cov}_\phi(x, y) - \mathrm{Cov}_{\phi_\infty}(x_0, y_0, x_0 + x, y_0 + y)\right| \leq \xi. \tag{13}$$

It is obvious that the *splicing* function defined here satisfies the first condition. The second condition requires the *splicing* function to be *normalized* in the whole region, and for the third condition, we have

$$\begin{aligned} &\left|\mathrm{Cov}_\phi(x, y) - \mathrm{Cov}_{\phi_\infty}(x_0, y_0, x_0 + x, y_0 + y)\right| \\ &\quad = \left|\mathrm{Cov}_\phi(x, y) - \mathrm{Cov}_\phi(x, y) \sum_{j=0}^{+\infty} \psi_j(x_0)\psi_j(x_0 + x)\right| \\ &\quad = \left|\mathrm{Cov}_\phi(x, y)\right| \cdot \left|1 - \sum_{j=0}^{+\infty} \psi_j(x_0)\psi_j(x_0 + x)\right|. \end{aligned} \tag{14}$$

When the point (0, 0) and the point (x_0, y_0) lies in the region with $\psi_j = 1$, $\left|1 - \sum_{j=0}^{+\infty} \psi_j(x_0)\psi_j(x_0 + x)\right|$ equals zero and it is evident that the *splicing* function satisfies condition three. When the point (x_0, y_0) lies in the 'cross region' and the point (0, 0) lies in the region with $\psi_j = 1$ or vice versa, $\left|1 - \sum_{j=0}^{+\infty} \psi_j(x_0)\right|$ is less than $\left|1 - \sum_{j=0}^{+\infty} \psi_j(x_0)\psi_j(x_0 + x)\right|$ for any *spilicing* functions, because of the second condition. We will discuss the maximum of equation (14) where (0, 0) and (x_0, y_0) are both in the 'cross region' below,

$$\begin{aligned} &\left|\mathrm{Cov}_\phi(x, y)\right| \cdot \left|1 - \sum_{j=0}^{+\infty} \psi_j(x_0)\psi_j(x_0 + x)\right| \\ &\quad = \left|\mathrm{Cov}_\phi(x, y)\right| \cdot \left|1 - \sum_{j=0}^{+\infty} \cos\left(\frac{\pi x}{2(p - 0.5 \cdot L_0)}\right)\right. \\ &\qquad \left. \times \cos\left(\frac{\pi(x_0 + x)}{2(p - 0.5 \cdot L_0)}\right)\right|. \end{aligned} \tag{15}$$

Expanding the cosine function into a second-order Taylor series, the following inequality holds:

$$\begin{aligned} &\left|\mathrm{Cov}_\phi(x, y) - \mathrm{Cov}_\phi(x, y) \sum_{j=0}^{+\infty} \psi_j(x_0)\psi_j(x_0 + x)\right| \\ &\quad \leq \left|\mathrm{Cov}_\phi(x, y)\right| \frac{\pi^2 x^2}{8(p - 0.5 \cdot L_0)^2}. \end{aligned} \tag{16}$$

The above inequality was also obtained in Vorontsov's paper and according to the conclusion of that paper, $\mathrm{Cov}_\phi(x, y)/\mathrm{Cov}_\phi(0, 0) < 0.0043$ for $x \geq L_0$. That means the error brought by the *splicing* function is less than a finite constant which is acceptable for real applications. For long phase screens with intermittency (not only with variable r_0 and L_0, but also with a variable spectrum model), we will calculate the sample lists according to our error

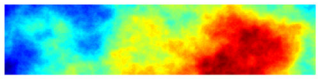

(a) A long phase screen of 20 meters long and 5 meters wide.

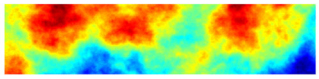

(b) A long phase screen of 20 meters long and 5 meters wide.

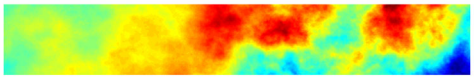

(c) A new phase screen (30m by 5m) generated by the combination of the above screens.

Figure 5. An example of generating a longer phase screen from two shorter ones.

requirements and simulate the phase screen with the above method. The addition of two phase screens with different outer scales (L_0) does not pose a problem if we use the smaller L_0 in equation (11). As an example, Fig. 5 shows a long phase screen generated by two shorter ones.

5.2 Atmospheric turbulence phase screen simulation for laboratory testing of AO systems

There are two main types of devices that can be used to simulate atmospheric turbulence phase screens in laboratory: a liquid crystal SLM and phase screens generated on fused silica using multilevel lithographic techniques. These are diffractive optical elements (DOEs) and generate phase screens with discrete step levels. The accuracy for the simulation depends on the levels of the discretization. An SLM typically has 2^8 grey levels, and there are typically five to eight binary photomasks for the lithographic technique. For SLMs with a stroke (maximum phase change) of 2π rad, the minimum accuracy for the phase screens is $2\pi/256 = 0.0245$ rad. For the phase screens generated by the multilevel lithographic technique, the minimum accuracy can be calculated:

$$\delta\phi = \frac{(n-1)\cdot d}{N\cdot\lambda}, \tag{17}$$

where n is the refractive index of the material, d is the thickness of the phase screen, λ is the wavelength, and N is the number of the binary photomasks. Because the phase screens generated with the optimal sampled sparse spectrum model have a controllable error, we can calculate the sampling lists corresponding to the physical simulation devices and generate the appropriate phase screen.

6 CONCLUSIONS

In this paper, we have demonstrated a new, unique method to simulate the atmospheric turbulence phase screens for large telescopes and stellar optical interferometers. With a controllable error budget, we have shown that our method can find the optimal sample list for different turbulent spectrum models, allowing the modelling of any power spectrum. Additionally, phase screens generated with our optimal sample list using a sparse spectrum model have improved statistical properties for a given computational requirement. We have also considered some real applications requiring phase screens and propose a method to connect site testing results with the fabrication and simulation of phase screens. This method is particularly suitable for simulation of AO systems of extremely large telescopes and stellar interferometers where the spectrum model is still an open question due to lack of sufficient data.

ACKNOWLEDGEMENTS

This work is funded by the Qualified Personnel Foundation of Taiyuan University of Technology (no: tyutrc-2013232), Shanxi Natural Science Foundation (Grant no. 2013011006-4), Lab of Adaptive Optics Foundation (Grant no. LAOF201301). The author would like to thank Chong Pei and Hualin Chen for their helpful discussions.

REFERENCES

Arcidiacono C., Diolaiti E., Tordi M., Ragazzoni R., Farinato J., Vernet E., Marchetti E., 2004, App. Opt., 43, 4288
Assémat F., Wilson R., Gendron E., 2006, Opt. Express, 14, 988
Babcock H. W., 1953, PASP, 65, 229
Basden A., 2014, MNRAS, 439, 2854
Basden A., Butterley T., Myers R., Wilson R., 2007, App. Opt., 46, 1089
Beghi A., Cenedese A., Masiero A., 2008, J. Opt. Soc. Am., 25, 515
Bonaccini D., Rigaut F. J., Glindemann A., Dudziak G., Mariotti J.-M., Paresce F., 1998, in Bonaccini D., Tyson R. K., eds, Proc. SPIE Conf. Ser. Vol. 3353, Adaptive Optical System Technologies. SPIE, Bellingham, p. 224
Bracewell R. N., 1986, The Fourier Transform and its Applications, 2nd edn. McGraw-Hill, New York
Burckel W. P., Gray R. N., 2013, App. Opt., 52, 4672
Cai D., Wang K., Jia P., Wang D., Liu J., 2014, Acta Phys. Sin., 63, 104217
Carbillet M., Riccardi A., 2010, App. Opt., 49, G47
Carbillet M. et al., 2004, in Bonaccini Calia D., Ellerbroek B. L., Ragazzoni R., eds, Proc. SPIE Conf. Ser. Vol. 5490, Advancements in Adaptive Optics. SPIE, Bellingham, p. 637
Charnotskii M., 2013, J. Opt. Soc. Am., 30, 479
Dekany R. G., Britton M. C., Gavel D. T., Ellerbroek B. L., Herriot G., Max C. E., Veran J.-P., 2004, in Bonaccini Calia D., Ellerbroek B. L., Ragazzoni R., eds, Proc. SPIE Conf. Ser. Vol. 5490, Advancements in Adaptive Optics. SPIE, Bellingham, p. 879
Fischer R. E., Tadic-Galeb B., Yoder P. R., 2008, Optical System Design, 2nd edn. McGraw-Hill, New York
Frehlich R., 2000, App. Opt., 39, 393
Frisch U., 1995, Turbulence. The Legacy of A. N. Kolmogorov. Cambridge Univ. Press, Cambridge
Greengard L., Lee J.-Y., 2004, SIAM Rev., 46, 443
Harding C. M., Johnston R. A., Lane R. G., 1999, App. Opt., 38, 2161
Hu L., Xuan L., Cao Z., Mu Q., Li D., Liu Y., 2006, Opt. Express, 14, 11911
Jia P., Zhang S., 2012, Res. Astron. Astrophys., 12, 584
Jolissaint L., Véran J.-P., Conan R., 2006, J. Opt. Soc. Am., 23, 382
Lane R. G., Glindemann A., Dainty J. C., 1992, Wave Random Media, 2, 209
Lloyd-Hart M., Angel R., Milton N. M., Rademacher M., Codona J., 2006, in Ellerbroek B L., Bonaccini Calia D., eds, Proc. SPIE Conf. Ser. Vol. 6272, Design of the Adaptive Optics Systems for GMT. SPIE, Bellingham, p. 62720E
Maire J., Ziad A., Borgnino J., Martin F., 2008, MNRAS, 386, 1064
Markus K.-P., 2010, in Clénet Y., Conan J.-M., Fusco Th., Rousset G., eds, Proc. 1st AO4ELT Conf., Adaptative Optics for Extremely Large Telescopes. EDP Sciences, Les Ulis, p. 01001
Martinez P., Kolb J., Sarazin M., Tokovinin A., 2010, The Messenger, 141, 5
Potter L. C., Arun K. S., 1989, IEEE Trans. Acoust. Speech Signal Process., 37, 1027

Recolons J., Dios F., 2005, in Doss-Hammel S. M., Kohnle A., eds, Proc. SPIE Conf. Ser. Vol. 5891, Atmospheric Optical Modelling, Measurement, and Simulation. SPIE, Bellingham, p. 51
Roddier F., 1981, in Van Heel A. C. S., ed., Progress in Optics, Vol. 19. North-Holland, Amsterdam, p. 281
Roddier N., 1990, Opt. Eng., 29, 1174
Sedmak G., 2004, App. Opt., 43, 4527
Sun W., Yuan Y.-X., 2006, Optimization Theory and Methods: Non-linear Programming, Vol. 1. Springer-Verlag, Berlin
Tatarskii V. I., 1961, Wave Propagation in Turbulent Medium. McGraw-Hill, New York
ten Brummelaar T. A. et al., 2012, in Ellerbroek B. L., Marchetti E., Véran J.-P., eds, Proc. SPIE Conf. Ser. Vol. 8447, Adaptive Optics Systems III. SPIE, Bellingham, p. 84473I
Tokovinin A., Sarazin M., Smette A., 2007, MNRAS, 378, 701
Vorontsov A. M., Paramonov P. V., Valley M. T., Vorontsov M. A., 2008, Wave Random Complex Media, 18, 91
Wu H.-L., Yan H.-X., Li X.-Y., Li S.-S., 2009, Opt. Express, 17, 14649
Xiang J., 2012, Opt. Express, 20, 681
Xiang J., 2014, Opt. Eng., 53, 016110
Xue B., Cui L., Xue W., Bai X., Zhou F., 2011, J. Opt. Soc. Am., 28, 912
Ziad A., Conan R., Tokovinin A., Martin F., Borgnino J., 2000, App. Opt., 39, 5415

This paper has been typeset from a TEX/LATEX file prepared by the author.